Human Bone Marrow–Derived Mesenchymal Stem Cells for Intravascular Delivery of Oncolytic Adenovirus Δ24-RGD to Human Gliomas

Raymund L. Yong,[1,4,5] Naoki Shinojima,[1,4] Juan Fueyo,[2,4] Joy Gumin,[1,4] Giacomo G. Vecil,[1,4] Frank C. Marini,[3] Oliver Bogler,[1,4] Michael Andreeff,[3] and Frederick F. Lang[1,4]

Departments of [1]Neurosurgery, [2]Neuro-oncology, and [3]Stem Cell Transplantation and [4]Brain Tumor Center, The University of Texas M. D. Anderson Cancer Center, Houston, Texas and [5]Division of Neurosurgery, Department of Surgery, The University of British Columbia, Vancouver, British Columbia, Canada

Abstract

Δ24-RGD is an infectivity-augmented, conditionally replicative oncolytic adenovirus with significant antiglioma effects. Although intratumoral delivery of Δ24-RGD may be effective, intravascular delivery would improve successful application in humans. Due to their tumor tropic properties, we hypothesized that human mesenchymal stem cells (hMSC) could be harnessed as intravascular delivery vehicles of Δ24-RGD to human gliomas. To assess cellular events, green fluorescent protein–labeled hMSCs carrying Δ24-RGD (hMSC-Δ24) were injected into the carotid artery of mice harboring orthotopic U87MG or U251-V121 xenografts and brain sections were analyzed by immunofluorescence for green fluorescent protein and viral proteins (E1A and hexon) at increasing times. hMSC-Δ24 selectively localized to glioma xenografts and released Δ24-RGD, which subsequently infected glioma cells. To determine efficacy, mice were implanted with luciferase-labeled glioma xenografts, treated with hMSC-Δ24 or controls, and imaged weekly by bioluminescence imaging. Analysis of tumor size by bioluminescence imaging showed inhibition of glioma growth and eradication of tumors in hMSC-Δ24-treated animals compared with controls ($P < 0.0001$). There was an increase in median survival from 42 days in controls to 75.5 days in hMSC-Δ24-treated animals ($P < 0.0001$) and an increase in survival beyond 80 days from 0% to 37.5%, respectively. We conclude that intra-arterially delivered hMSC-Δ24 selectively localize to human gliomas and are capable of delivering and releasing Δ24-RGD into the tumor, resulting in improved survival and tumor eradication in subsets of mice. [Cancer Res 2009;69(23):8932–40]

Introduction

Current treatments for glioblastoma, the most common adult malignant brain tumor, result in a median survival of only 14 months (1). However, recent evidence has shown that Δ24-RGD, a tumor-selective, replication-competent adenovirus with augmented cellular infectivity, may be effective against this fatal disease (2, 3). Because it contains a mutant viral E1A gene, Δ24-RGD selectively replicates in and lyses tumor cells in which the retinoblastoma protein is inactivated. The augmented infectivity of Δ24-RGD is due to an insertion of a RGD motif in the fiber knob, allowing for integrin-mediated infection, independent of cocksackie-adenovirus receptors (4, 5), which are minimally expressed in gliomas. In an orthotopic model of human gliomas, intratumoral injection of Δ24-RGD resulted in a significantly longer survival than controls (3).

Despite success in preclinical models, human gliomas in patients are heterogeneous, containing multiple barriers to viral spread that represent hurdles for successful virus-mediated tumor eradication after intratumoral injection (6–8). Intravascular delivery may overcome these barriers because it can produce widespread initial viral distribution in the tumor and repeat dosing is possible. Unfortunately, intravascular administration of adenovirus is limited by liver toxicity and neutralizing antibodies (8–10).

Recent evidence has shown that human bone marrow–derived mesenchymal stem cells (hMSC) are useful delivery vehicles for brain tumor therapy (11, 12). hMSCs are well suited for clinical applications because they are easily obtained from patients, their procurement poses no ethical concerns, and autologous transplantation is possible (13, 14). We have shown that hMSCs selectively localize to human gliomas after intravascular administration, and they can deliver antiglioma agents to orthotopic models of the disease (11). Their capacity to localize to gliomas may reflect an intrinsic ability of MSCs to home to most solid tumors (15–18).

Previous work using hMSCs to deliver oncolytic adenoviruses to tumors has met with some success (19–21). However, these studies have provided limited information about the cellular events underlying the intravascular delivery of oncolytic viruses via hMSCs. The effects of Δ24-RGD on the tropism of hMSCs for gliomas after intravascular delivery remain unknown. Moreover, it is unclear whether hMSCs loaded with Δ24-RGD are capable of lysing and releasing the virus once within gliomas. Because hMSCs express normal retinoblastoma protein, a priori one would not expect Δ24-RGD to replicate in hMSCs. However, there may be a window for viral replication during stem cell self-renewal during which retinoblastoma protein is inactivated. Lastly, no study has shown improvements in survival when MSCs are used to deliver viral therapies to gliomas. Although one report suggests that hMSCs carrying oncolytic viruses can migrate short distances toward brain tumors after juxtatumoral injection, efficacy was not shown, and the feasibility of intravascular delivery was not explored (22). Here, we address these issues and show for the first time that hMSCs are able to deliver Δ24-RGD to human gliomas after intravascular injection and that this strategy results in long-term survival in animal models of gliomas.

Note: Supplementary data for this article are available at Cancer Research Online (http://cancerres.aacrjournals.org/).

Requests for reprints: Frederick F. Lang, Department of Neurosurgery, Box 442, The University of Texas M. D. Anderson Cancer Center, 1515 Holcombe Boulevard, Houston, TX 77030. Phone: 713-792-2400; Fax: 713-794-4950; E-mail: flang@mdanderson.org.

doi:10.1158/0008-5472.CAN-08-3873

Materials and Methods

Mesenchymal stem cells. Male hMSCs were obtained from Lonza. Cells were positive for CD44, CD73, CD90, and CD105 and negative for CD34, CD45, and CD133. Cells were expanded in a 37°C, 5% CO_2 incubator in α-MEM containing 10% fetal bovine serum (Sigma), 1% 2 mmol/L L-glutamine (Invitrogen), and 1% penicillin-streptomycin (Lonza) and were used at passages 5 to 7.

Tumor cells. Glizoblastomas U87MG and LN229 were obtained from the American Type Culture Collection. D54 was provided by Darell Bigner (Duke University), and U251 and U251-V121 were provided by W.K. Alfred Yung (M. D. Anderson Cancer Center). Cells were grown in MEM-α containing 10% fetal bovine serum and 1% penicillin-streptomycin. U87MG-GL containing green fluorescent protein (*Gfp*) and luciferase were obtained from T.J. Liu (M. D. Anderson Cancer Center). U87MG-LucNeo, as described previously (23, 24), were provided by B.S. Carter (Massachusetts General Hospital) and grown in U87MG medium containing 0.5 mg/mL zeocin (Invitrogen). U87MG-XO karyotype cells were selected from U87MG by cloning single XO cells.

MSC labeling and infection. hMSCs were transduced with *Gfp* using a replication-incompetent Ad5/F35-CMV-GFP (Ad-GFP; ref. 25; Vector Development Laboratory, Baylor College of Medicine). Monolayers were treated with 50 multiplicities of infection (MOI) in 3 mL serum-free hMSC medium shaken every 10 min at 37°C. After 1 h, hMSC medium containing 10% fetal bovine serum was added. For infection with Δ24-RGD, 10 to 100 plaque-forming units/cell of viral stock solution were added to the 3 mL serum-free medium mixture containing Ad5/F35-CMV-GFP.

Cell cycle analysis. hMSCs (3×10^5) were cultured in serum-free medium for 72 h to synchronize cells. Cells were infected with Δ24-RGD at 0 (sham), 10, 50, and 100 MOIs in serum-free medium. At 1 h, α-MEM containing 10% fetal bovine serum was added and hMSCs were collected and fixed 24, 48, and 72 h later. Collected hMSCs were centrifuged and resuspended in 500 μL PBS. RNase A (Roche Applied Science) was added followed by propidium iodide (100 μL/mL cells; Roche Applied Science) and analyzed by flow cytometry.

Viral titering. hMSCs (2×10^5) were plated for 24 h and then infected with Δ24-RGD at various multiplicities over 1 h, after which growth medium was added. After infection, the medium was collected and cells were trypsinized and centrifuged. The collected medium was added to the pellet and cells were resuspended. Each sample was subjected to three freeze-thaw cycles to lyse hMSCs. After centrifugation, the titer in supernatant was determined using the Adeno-X RapidTiter kit (Clontech Laboratories).

***In vitro* efficacy testing.** Transwell experiments were done using 0.4 μm pore plates (Corning). hMSCs infected with various MOIs of Δ24-RGD were collected, washed, replated in the upper well at 1×10^4 cells per well, and placed over lower wells containing glioma cells (3×10^4 cells per well). After 7 days, viable glioma cells were counted using an automated hemocytometer.

Animals. Male athymic mice (*nu/nu*; Department of Experimental Radiation Oncology, M. D. Anderson Cancer Center) were manipulated according to the institutional approved protocols and anesthetized using 0.25 mL of 10 mg/mL ketamine and 1 mg/mL xylazine cocktail, i.p.

Intracranial glioma xenograft implantation. Glioma cells were implanted via cranial guide screws as described previously (26). Mice received 5×10^5 (U87) or 1×10^6 (U251-V121) cells via a Hamilton syringe inserted to a depth of 5 mm. Ten mice were implanted simultaneously using a microinfusion syringe pump (0.5 μL/min; Harvard Apparatus) as described previously (11).

Internal carotid artery injection of MSCs. hMSCs were trypsinized, centrifuged (1,500 rpm, 5 min × 3), and resuspended in hMSC medium with 10% fetal bovine serum at 1×10^6 cells per 100 μL. Injection at the right carotid artery was done as described previously (27), except that a 30-gauge needle was used to inject cells.

Tissue preparation/fixation and immunostaining. Mice were sacrificed by intracardiac perfusion of PBS and 4%paraformaldehyde. Brains were removed, fixed in 10% formalin for 24 h, embedded in paraffin, and cut (5 μm sections). Detection of Δ24-RGD was done using mouse anti-hexon (1:100 dilution; Santa Cruz Biotechnology) and rabbit anti-E1A (1:200 dilution; Santa Cruz Biotechnology) antibodies. GFP-labeled hMSCs were detected with rabbit anti-GFP antibodies (1:200 dilution; Santa Cruz Biotechnology). Immunohistochemistry was done using the ImmPRESS Antibody kit (Vector Laboratories). Immunofluorescence used biotinylated secondary antibodies and fluorescein- or Texas red–conjugated avidin (Vector Laboratories).

Fluorescence *in situ* hybridization. Hybridization was done using dual-color subcentromeric probes for human X or Y chromosome (Vysis) according to the manufacturer's recommendations.

Bioluminescence imaging. Mice were imaged with Xenogen IVIS 200 system (Xenogen) after administering 4 mg D-luciferin i.p. Images were collected using exposure times between 0.1 s and 5 min. Bioluminescence imaging were overlaid on grayscale photographic images using Living Image 3.0 software (Xenogen). Data analysis was based on the total photon flux from a standard-sized region of interest.

Statistical analysis. Cell counts were expressed as mean ± SD. Comparisons were made using two-way ANOVA. Bioluminescence imaging data were analyzed using nonlinear regression based on an exponential growth model and compared using the extra sum-of-squares *F* test. Survival curves were compared using the log-rank test. Analyses were done using GraphPad Prism 5.01.

Results

Δ24-RGD infection and replication within hMSCs *in vitro*. Because our strategy involves *ex vivo* transduction of hMSCs, we investigated the extent to which Δ24-RGD is capable of infecting

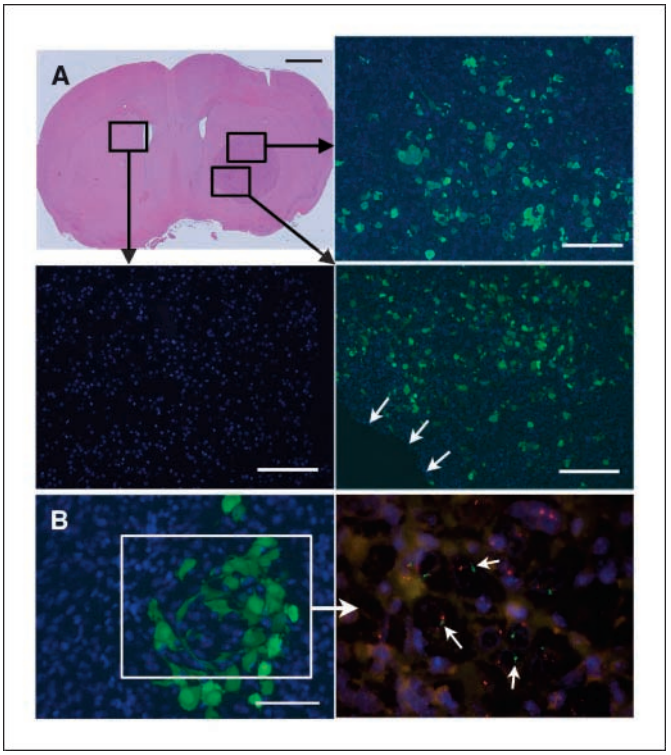

Figure 1. *A,* representative mouse implanted with U87MG in the right frontal lobe. One million GFP-labeled hMSCs were injected into the right carotid artery on day 7. The brain was extracted for histology on day 11. *Bar,* 1 mm. Boxed areas were subjected to immunofluorescence using anti-GFP antibodies to reveal the distribution of hMSCs (*green*) within the xenograft. *Blue,* 4′,6-diamidino-2-phenylindole nuclear dye. *B,* cluster of GFP-labeled hMSCs of genotype XY is seen within a U87MG xenograft of genotype XO after intracarotid delivery. *Bar,* 50 μm. The boxed area shows fluorescence *in situ* hybridization on an adjacent section to reveal Y chromosomes (*green*; *arrows*) within the area where hMSCs were present. Outside this area, only cells containing X chromosomes (*red*) are seen.

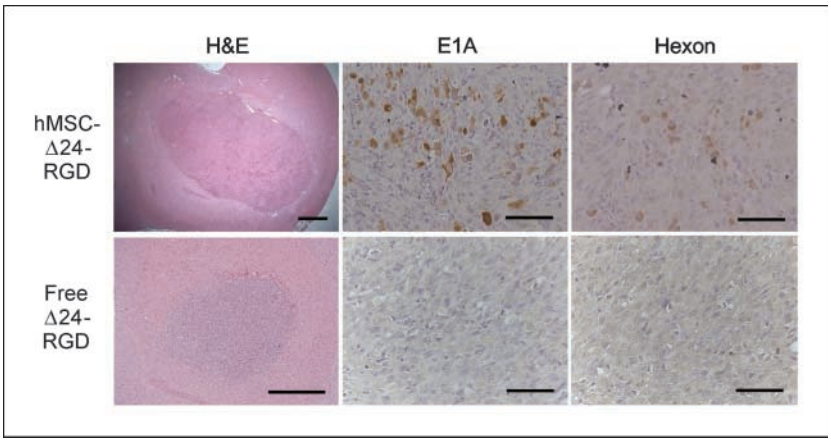

Figure 2. hMSC-Δ24 produces tumor infections, whereas free Δ24-RGD does not. Mice were treated as described in the text and brain sections were immunostained with anti-E1A or anti-hexon antibodies. Viral E1A protein and hexon protein were seen throughout hMSC-Δ24–treated brains (brown cytoplasmic stain) but not in controls treated with free virus. Additionally, E1A and hexon were absent in brains treated with uninfected hMSCs and PBS (data not shown). *Bar,* 500 μm (H&E sections) and 50 μm (immunostained sections).

hMSCs. hMSCs express integrins but lack cocksackie-adenovirus receptor (28); thus, we compared the infectivity of hMSCs by adenoviral vectors expressing or lacking the RGD motif and found increased infectivity Ad-RGD (Supplementary Fig. S1*A*). To verify this result for Δ24-RGD, we infected hMSCs with Δ24-RGD containing *Gfp* as a reporter (Δ24-RGD-GFP). More than 80% of hMSCs expressed GFP after 24 h (Supplementary Fig. S1*B*), and after 72 h, nearly all hMSCs exhibited cytopathic effect (Supplementary Fig. S1*C*). Because Δ24-RGD replicates poorly in cells with normal retinoblastoma protein pathways (2, 3), this result suggests that retinoblastoma protein in hMSCs is inactivated independently of adenoviral E1A when hMSCs spontaneously enter S phase, allowing hMSCs to support the replication of Δ24-RGD.

hMSCs carrying Δ24-RGD localize to human gliomas after intracarotid delivery. To determine the extent to which hMSCs carrying Δ24-RGD are capable of selectively localizing to gliomas after intravascular delivery *in vivo*, U87MG cells (5×10^5) were implanted into the frontal lobes of nude mice ($n = 6$). One day before delivery, hMSCs were transduced with Δ24-RGD (10 MOI) and Ad-GFP (50 MOI), generating hMSC-Δ24-Ad-GFP, and injected into the right carotid artery (1×10^6 cells per 100 μL medium) of mice harboring 7-day-old xenografts. Mice were sacrificed 4 days later (Fig. 1). Immunofluorescence staining with anti-GFP antibodies showed hMSCs throughout the tumors (Fig. 1*A*). Virtually no hMSCs were seen elsewhere in the brain. Similar results were obtained using U251-V121 xenografts (Supplementary Fig. S2). Sex-mismatched

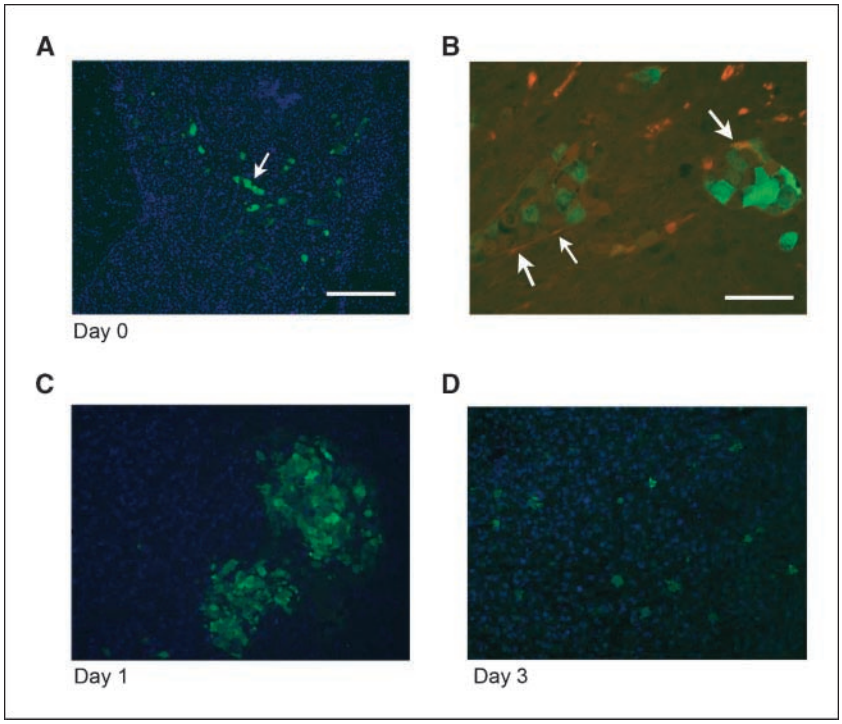

Figure 3. *A,* brain section from a mouse sacrificed immediately after hMSC delivery showing the presence of GFP-labeled hMSCs organized in linear patterns (*arrows*), suggesting arrival via tumor blood vessels. *Bar,* 200 μm. *B,* section from a separate mouse stained with antibodies against endothelial marker CD31 and GFP. GFP-positive cells (*green*) are hMSCs and CD31-positive cells (*red*) are endothelial cells. *Arrows,* area where red endothelial cells surround green hMSCs. *Bar,* 50 μm. *C* and *D,* mice were implanted with U87MG and then treated with hMSC-Δ24-RGD-Ad-GFP. Analysis of brains on days 1 and 3 by fluorescence microscopy after staining anti-GFP antibody (*green*) revealed hMSCs arranged in clusters on day 1 (*C*). By day 3, hMSCs had dispersed within the xenografts (*D*). *Blue,* 4′,6-diamidino-2-phenylindole.

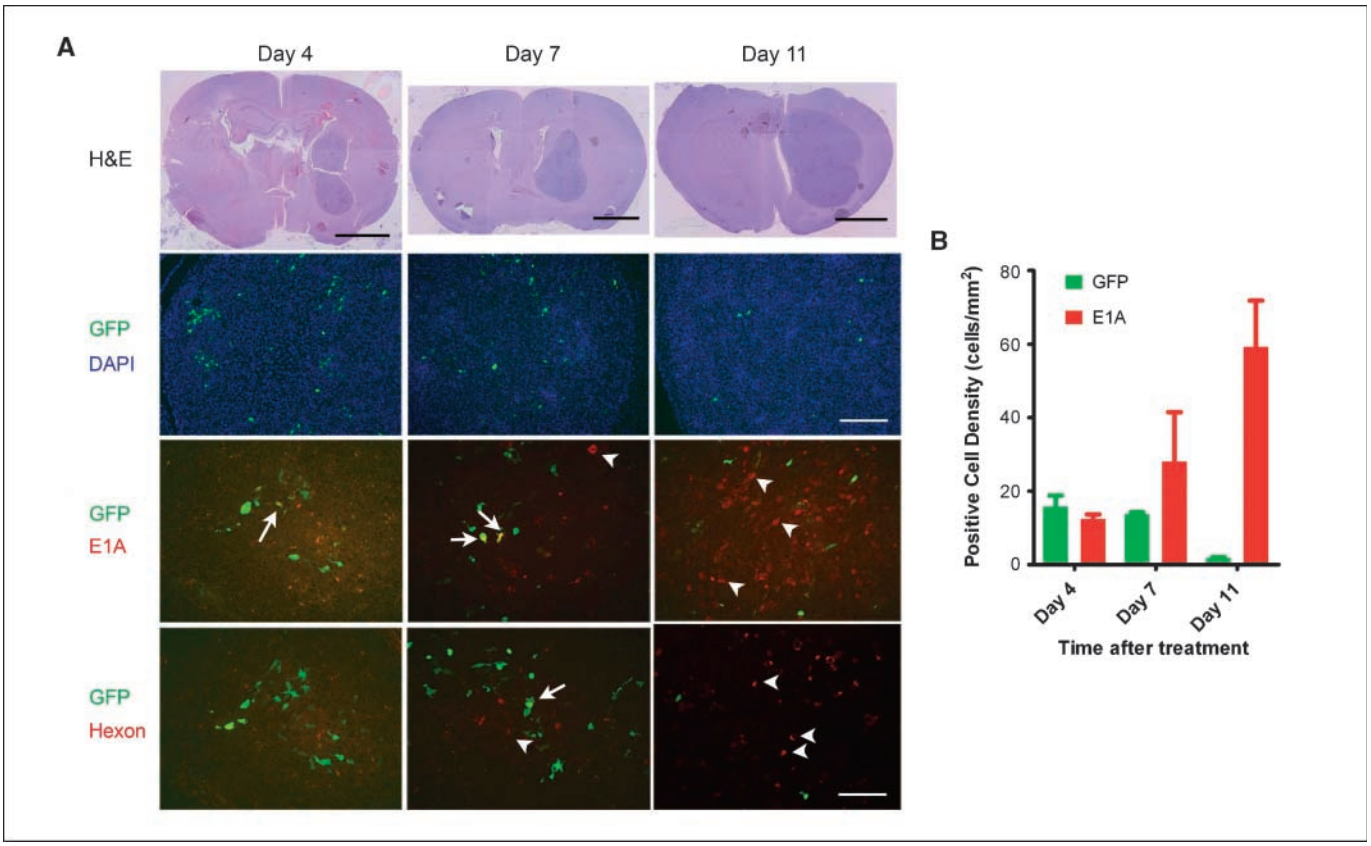

Figure 4. *A,* immunofluorescence microscopy was used to track hMSCs and Δ24-RGD over time after intracarotid delivery to U87MG xenografts. Brains were harvested 4, 7, and 11 d after treatment. Sections were cut and stained with H&E (*row 1*). Sections were double immunostained with FITC-labeled anti-GFP antibody (*green*) and Texas red–labeled anti-E1A antibody (*row 3*; *red*) or Texas red–labeled anti-hexon antibody (*row 4*; *red*). Sections were also stained with 4′,6-diamidino-2-phenylindole (*DAPI*; *row 2*). Green cells indicate hMSCs that are not expressing viral proteins, yellow cells indicate hMSCs that are expressing viral proteins, and red cells indicate U87 tumor cells expressing viral proteins. *Arrows,* examples of hMSC double-expressing GFP and E1A (*yellow cells*); *arrowheads,* examples of E1A-expressing U87MG cells (*red cells*). The pattern indicates progression from green to yellow to red cells, suggesting movement of virus from hMSCs to glioma cells. *Bar,* 2 mm (H&E), 200 μm (GFP/4′,6-diamidino-2-phenylindole), and 100 μm (EIA and hexon). *B,* density of GFP-positive cells (hMSCs) and adenoviral protein-expressing cells (cells supporting viral replication) within U87MG xenografts over the course of the experiment depicted in *A*. $P_{interaction}$ = 0.0006, two-way ANOVA.

transplant experiments using XO-genotype U87MG xenografts (see Materials and Methods) and male (XY) hMSCs confirmed that GFP-positive cells within the xenografts were hMSCs (Fig. 1*B*).

Δ24-RGD infection of xenografts requires hMSCs. To show that hMSCs are required for Δ24-RGD to infect gliomas after intravascular delivery, U87MG cells were implanted into the brains of nude mice. After 7 days, mice (n = 3 per group) were injected with 1×10^6 hMSC-Δ24 (transduced with 10 MOI 24 h before injection) or 1×10^8 cell-free Δ24-RGD viral particles. Seven days later, brains were analyzed by immunohistochemistry for adenoviral E1A and hexon proteins (Fig. 2). Viral protein expression was seen only after treatment with hMSC-Δ24, indicating that effective delivery of Δ24-RGD to gliomas requires packaging within hMSCs.

Initial localization of hMSC-Δ24 in gliomas. We next sought to define the cellular events underlying the delivery of Δ24-RGD by hMSCs. U87MG cells (5×10^5) were implanted into the brains of mice, and after 7 days, hMSC-Δ24-Ad-GFP were injected into the right internal carotid artery (1×10^6 cells). Immunofluorescence staining with anti-GFP antibodies of tumors harvested immediately (within 1 h) after injection (n = 3) showed GFP-labeled hMSCs within the xenografts in linear arrangements, suggesting an intravascular location (Fig. 3*A*). Consistent with this interpretation, double immunofluorescence staining for endothelial marker PECAM1(CD31) and GFP indicated that GFP-labeled hMSCs were located within tumor vessels (Fig. 3*B*). To further decipher the pattern of spread of hMSC-Δ24, xenografts were analyzed 1 to 3 days after hMSC delivery (n = 3 per time point). GFP-labeled hMSCs were found in clusters until day 2 (Fig. 3*C*), after which they were dispersed through the tumor (Fig. 3*D*). Together, these results suggest that hMSC-Δ24 localized to gliomas via the vasculature and then migrated into the tumor parenchyma.

Spread of Δ24-RGD from hMSCs into glioma cells. To elucidate the spread of Δ24-RGD after arrival of hMSC-Δ24 in xenografts, we analyzed specimens treated with intravascularly delivered hMSC-Δ24 using FITC-conjugated antibody against GFP to track hMSC-Δ24-Ad-GFP and Texas red–conjugated anti-E1A (or anti-hexon) antibody to track Δ24-RGD (Fig. 4). Mice (n = 3 per time point) were implanted with U87MG xenografts and after 7 days were treated with 1×10^6 hMSC-Δ24-Ad-GFP (10 MOI for 24 h). Animals were sacrifice 4, 7, and 11 days after treatment. Immunofluorescence using a FITC-conjugated antibody against GFP revealed GFP-labeled hMSCs (green) throughout the xenografts at day 4 and fewer hMSCs at day 7. By day 11, only rare hMSCs were detected, suggesting that hMSC-Δ24 were lysed over time. In comparison, control mice injected with hMSC-Ad-GFP (without Δ24-RGD) showed hMSCs within xenografts 14 days after

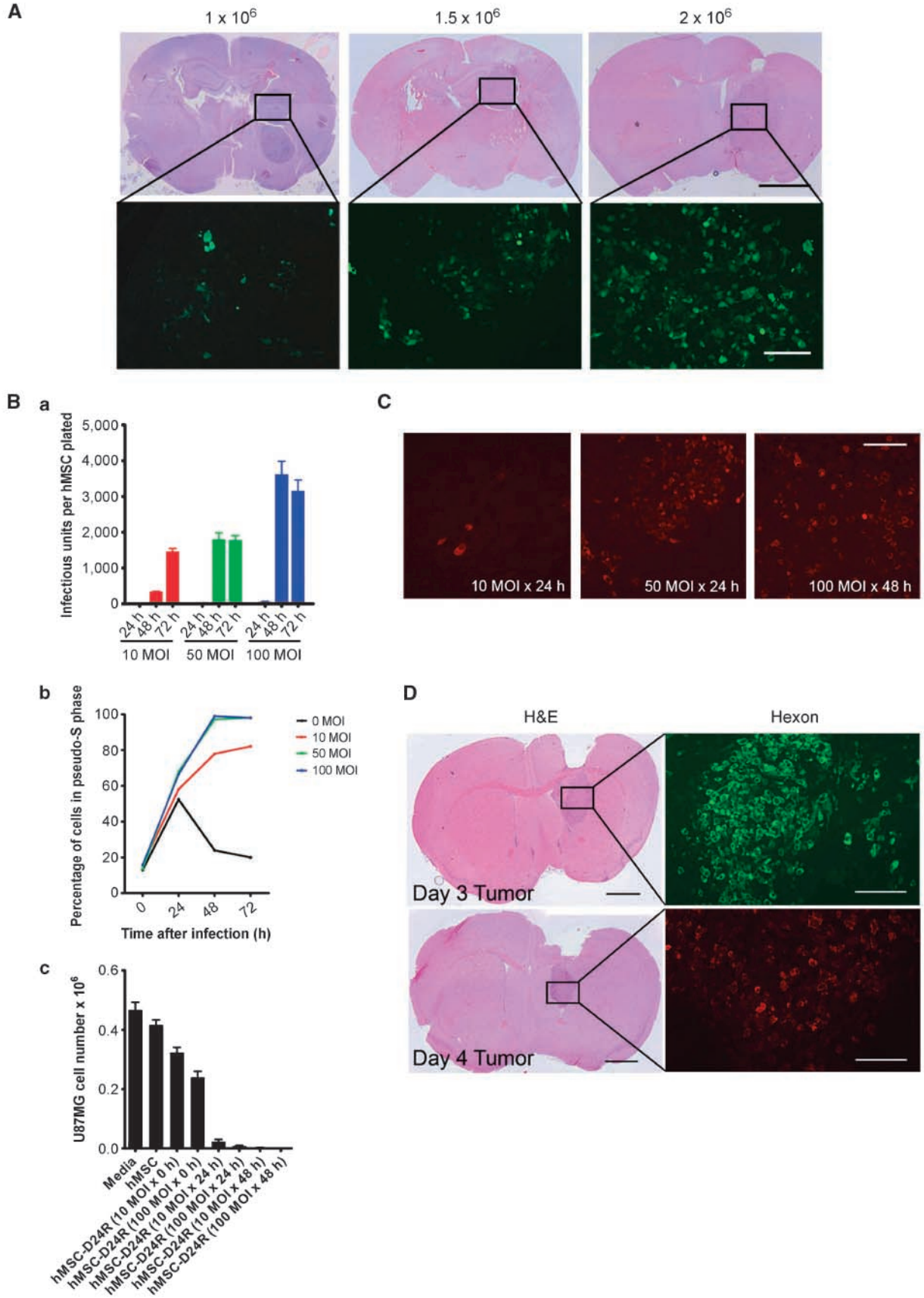

injection (data not shown). Immunofluorescence using Texas red–conjugated anti-E1A or anti-hexon antibodies to track expression or Δ24 viral proteins showed that E1A and hexon (red staining) was rare on day 4, increased on day 7, and was abundant on day 11. When merged images were analyzed after double staining with FITC–anti-GFP antibody and Texas red–anti-E1A (or anti-hexon antibody), green cells (indicative of hMSCs) were abundant on day 4 and yellow cells (indicative of viral replication within hMSCs) were evident on day 4 and increased by day 7. By day 11, red cells (indicative of U87 tumor cells expressing viral proteins) dominated the images (Fig. 4*A*). Taken together, these findings suggest that Δ24-RGD replicated within hMSCs, was released from lysed hMSCs, and subsequently infected U87MG tumor cells. Hexon expression lagged behind E1A expression, as expected. Control mice injected with hMSC-GFP exhibited no evidence of adenoviral protein expression at any time (data not shown).

To quantify these results, the number of GFP-positive and E1A-positive cells were counted on at least five tissue sections per mouse and the cell density was determined by dividing the cell count by the cross-sectional area of the xenograft (Fig. 4*B*). E1A expression (viral replication) increased significantly over time, whereas GFP expression (hMSCs) decreased ($P = 0.0006$, two-way ANOVA).

To verify that these results were not unique to U87MG xenografts, similar experiments were carried out using U251-V121 glioma cell lines. In these experiments hMSCs were infected with 50 MOI Δ24-RGD and 50 MOI Ad5/F35-CMV-GFP and injected into the carotid arteries of U251-V121–bearing mice. Similar to U87 gliomas, hMSC-Δ24 localized to U251-V121 and supported the replication and release of Δ24-RGD (Supplementary Fig. S3*A*). Quantification of the result showed progressive loss of hMSCs and increase in viral infection of U251-V121. However, the time course in U251-V121 was slightly accelerated compared with U87MG probably due to the infection of hMSCs with a higher amount of Δ24-RGD (50 versus 10 MOI; Supplementary Fig. S3*B*).

Optimization of viral yield: *in vitro* efficacy experiments. We next sought to improve the efficiency of this approach. We administered increasing doses of GFP-labeled hMSCs to glioma-bearing mice and found that this produced increasing numbers of engrafted cells (Fig. 5*A*). Because injection of 2×10^6 cells resulted in deaths due to respiratory failure from cells arriving in the lungs (Supplementary Fig. S4), a dose of 1.5×10^6 hMSCs was used for *in vivo* efficacy experiments.

We then titered the total amount of Δ24-RGD produced by hMSCs at 10, 50, and 100 MOI *in vitro* after 24, 48, and 72 h and found maximal adenoviral production at 48 h using 100 MOI (Fig. 5*B, a* and *b*). Because by many hMSCs exhibited cytopathic effect, we deduced that delivery of hMSCs 48 h after infection with Δ24-RGD (100 MOI) would avoid loss of virions from premature release and maximize the number of replicated virions available for tumor infection.

A Transwell assay confirmed that hMSCs release viable Δ24-RGD that is then capable of infecting and killing U87MG cells *in vitro* (Fig. 5*B, c*). Other glioma cell lines (D54, LN229, U251, and U251-V121) were also found susceptible to hMSC-Δ24 in this Transwell assay (Supplementary Fig. S5).

Corresponding *in vivo* experiments showed higher levels of hexon expression after 4 and 7 days in U87MG xenografts when hMSCs were incubated at 50 MOI for 24 h and at 100 MOI for 48 h compared with incubating at 10 MOI for 24 h ($n = 3$ animals per group; Fig. 5*C* and *D*). Based on these experiments, hMSCs were transduced by incubating with 50 MOI Δ24-RGD for 24 h in all *in vivo* efficacy experiments.

hMSC-Δ24 inhibit xenograft growth and improve survival. To determine whether hMSC-Δ24 is efficacious against gliomas *in vivo*, two independent experiments were done (Fig. 6), in which mice received 1.5×10^6 hMSC-Δ24 (50 MOI × 24 h) via carotid artery injection 4 and 18 days after xenograft implantation. Two different luminescent U87MG cell lines (U87MG-GL in Fig. 6*A, a* and *B, a*, and U87MG-LucNeo in Fig. 6*A, b* and *B, b*) were used. Bioluminescence imaging showed marked differences in photon flux among the groups by 5 weeks in experiment 1 (Fig. 6*C*) and 3 weeks in experiment 2 (Supplementary Fig. S6*A*). Nonlinear regression using an exponential growth model showed significant differences in the rate constants for the control and treatment arms in both experiments (experiment 1: $P < 0.0001$ and experiment 2: $P = 0.0005$, extra sum-of-squares F test; Supplementary Fig. S6*B* and *C*). Furthermore, survival analyses showed a significant improvement in median survival from 42 to 75 days in experiment 1 and 45 to 60 days in experiment 2 ($P < 0.01$, log-rank test, for all comparisons; Fig. 6*B*). Survival beyond 80 days in the hMSC-Δ24 groups was 37.5% in experiment 1 and 36% in experiment 2 compared with 0% in the control groups. Analysis of the brains of animals living beyond 120 days revealed no residual tumors (Supplementary Fig. S7).

Discussion

Previous studies employing hMSCs carrying oncolytic adenoviruses to pulmonary metastases, soft-tissue tumors, and gliomas have shown limited numbers of hMSCs and adenoviral antigen-expressing cells inside the tumors (19, 20, 22). Efficacy of hMSC-based oncolytic viral therapy in glioma models after local delivery has not been shown, and heretofore no study has attempted

Figure 5. Optimization of delivery of Δ24-RGD to U87MG xenografts via hMSCs. *A,* an increased number of delivered hMSCs correlates with an increased number of engrafted hMSCs. Mice were implanted with 5×10^5 U87MG cells in the right frontal lobe and allowed to grow for 7 d. GFP-labeled hMSCs (1.0, 1.5, or 2×10^6) were injected into the carotid artery. Mice were sacrificed 4 d later. *Bar,* 2 mm (H&E) and 100 μm (hMSC-GFP). *B, a,* hMSCs were infected with Δ24-RGD at 10, 50, or 100 MOI and allowed to incubate for 24, 48, or 72 h. Cells were collected along with medium and the titer of Δ24-RGD was measured to determine the number of infectious units released. The highest number of infectious units was obtained using 100 MOI incubated for 48 h. Experiment done in triplicate. *b,* hMSCs were plated in serum-free medium and allowed to synchronize. At 0 h, cells were infected with Δ24-RGD at 0, 10, 50, or 100 MOI. At the indicated time points, cell cycle analysis was done. Results are the percentage of cells in S phase or pseudo-S phase. All hMSCs infected with 50 or 100 MOI exhibited evidence of viral DNA replication by 48 h. *c,* hMSCs were infected with Δ24-RGD at the indicated MOIs and then washed and plated in the upper wells of a Transwell plate (1×10^4 cells per well). U87MG cells were plated in the bottom wells (3×10^4 cells per well) and incubated for 7 d, after which U87MG cells were counted. Killing was seen with ≥10 MOIs and incubation times of ≥24 h. *C,* mice were implanted with U87MG cells and treated with hMSC-Δ24 at the indicated MOIs and incubation times. Four days later, brains were analyzed by immunofluorescence for hexon protein expression (*red cells*). The 50 MOI × 24 h and 100 MOI × 48 h incubations produced equivalent infections. *Bar,* 100 μm. *D,* mice were implanted with U87MG cells and injected with 1.5×10^6 hMSC-Δ24 (50 MOI × 24 h incubation) 3 d (*top*) or 4 d (*bottom*) later. On day 7 after delivery of hMSCs, xenografts were analyzed for hexon protein expression (*green* in *top* and *red* in *bottom*). *Bar,* 1 mm (H&E) and 200 μm (hexon).

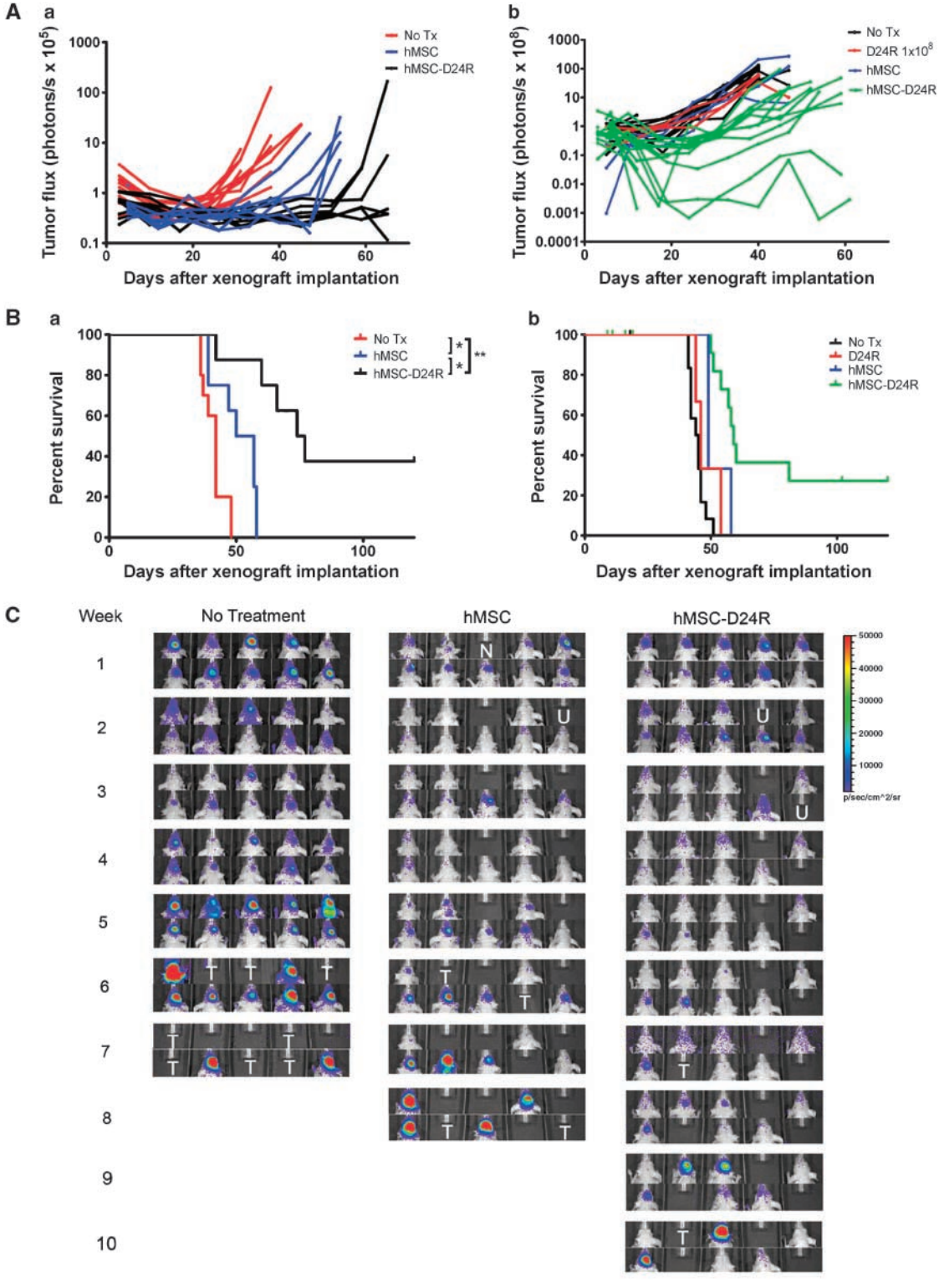

Figure 6. *A,* photon flux of xenografts over 60 d for two independent experiments in which nude mice were implanted with luminescent U87MG xenografts (U87MG-GL in *a* and U87MG-LucNeo in *b*; 5×10^5 cells). In each experiment, 10 mice were left untreated and 10 to 20 mice underwent two treatments with "empty" hMSCs or hMSC-Δ24 (1.5×10^6 cells; 50 MOI × 24 h incubation). Mice were imaged weekly. Total photonic flux was measured from fixed regions of interest encompassing the entire head. Each line represents efflux from a single animal. Slower growth is seen with hMSC-Δ24 treatment. *B,* survival data corresponding to the two experiments presented in *A*. In experiment 1 (*a*), median survival was 77 d in treated animals compared with 42 d in untreated controls and 53.5 d in animals given "empty" hMSCs. Among treated animals, 37.5% lived beyond 80 d. *, $P < 0.01$; **, $P = 0.0002$, log-rank test. In experiment 2 (*b*), median survival was 60 d in treated animals compared with 45 d in untreated controls. Thirty-six percent of animals lived beyond 80 d. ***, $P < 0.0001$, log-rank test. *C,* representative bioluminescence images over the time course of the experiment depicted in *A*. Individual mice were tracked. *N,* no animal; *U,* death unrelated to tumor; *T,* tumor-related death.

intravascular delivery. Thus, the results presented here elucidate for the first time the cellular events underpinning hMSC-mediated delivery of Δ24-RGD to human gliomas and show that hMSC-Δ24 are effective antiglioma agents after intravascular delivery.

Several investigators have raised concerns that intravascularly delivered hMSCs might not reach gliomas due to the blood-brain/tumor barrier (22). However, we show that hMSC-Δ24 localize to gliomas, probably via the tumor vasculature, and migrate into the tumor. Our findings are consistent with studies of inflammation where hMSCs participate in adhesion and transmigration cascades similar to leukocytes (29–31). Whether similar mechanisms are operant in gliomas requires further investigation.

We found that, after arriving within the tumor, the number of GFP-labeled hMSCs decreased over time, whereas adenoviral E1A and hexon expression increased (see Fig. 4). E1A and hexon expression was first found in GFP-positive hMSCs and then in non-GFP-labeled glioma cells. Together, these results suggest that Δ24-RGD replicates in hMSCs, is released through lysis of hMSCs, and then infects glioma cells. These findings are consistent with Stoff-Khalili and colleagues who showed hexon within intratumoral hMSCs carrying Ad5/3.CXCR4 after i.v. delivery to pulmonary breast metastases (20). However, their studies did not define how hMSCs reached the tumors or whether the virus infected tumor cells. Other studies did not track hMSCs and adenoviral activity simultaneously (19, 21, 22). Therefore, to our knowledge, our studies are the first to specifically track the progress of Δ24-RGD from hMSC to the tumor cells.

We show that the timing of intravascular delivery of hMSCs in relation to their infection with Δ24-RGD *ex vivo* is critical for optimizing viral yield *in vivo*. By delivering hMSCs 24 to 48 h after infection with Δ24-RGD, we were able to achieve robust tumor infection. This supports the concept that hMSCs can be harnessed as "factories" to amplify oncolytic adenoviruses (20). Viral replication appears to exploit the capacity of hMSC to self-renew, inducing inactivation of retinoblastoma protein as hMSCs enter S phase. Viral titering experiments indicated that each hMSC can produce ~2,000 virions after infection with 50 MOI. We estimate that 1,000 hMSCs localize to our xenografts (data not shown). Thus, $\sim 2 \times 10^6$ virions are potentially released into the tumor after a single injection. Only intravascular doses above a threshold of 1×10^{10} adenoviral particles are capable of saturating viral clearance mechanisms to produce sufficient levels of viremia to enable tumor infection (32). In contrast, single intratumoral injections of only 1×10^7 viral particles of Δ24-RGD have been shown to retard glioma growth (33). Thus, packaging Δ24-RGD within hMSCs is a more efficient means of infecting tumors with Δ24-RGD than intravascular injection of free virus and is at least as efficient as intratumoral delivery.

The dense xenograft infections elicited by hMSC-Δ24 in our animal models ultimately translated into an antiglioma effect and prolonged animal survival. Long-term survival rates of 30% to 40% were achieved, and cures were shown at 120 days. These results are comparable with Fueyo and colleagues who achieved a 60% long-term survival rate after administering a total of 4.5×10^8 plaque-forming units Δ24-RGD divided over three intratumoral injections (3, 33). In comparison, we administered a total of 3×10^6 hMSC-Δ24 divided over two intravascular injections, which resulted in an estimated total dose of $<1 \times 10^7$ plaque-forming units Δ24-RGD. Because hMSC-based intravascular delivery is disseminated within tumors, rather than focused at a single site as occurs with local injection, the smaller dose delivered by hMSCs was sufficient to produce a therapeutic effect comparable with intratumoral injection. Further benefit is potentially achievable by additional intravascular injections of hMSC-Δ24, which are technically difficult in small animals but feasible in patients using endovascular techniques.

Questions remain about possible adverse effects of hMSC-Δ24. Because mice are not a natural host for adenovirus, they do not support replication of Δ24-RGD; therefore, assessments of adverse effects of Δ24-RGD could not be ascertained in our models. Cotton rats or Syrian hamsters, the only nonhuman species that support adenoviral replication, are needed to specifically evaluate the toxicity of Δ24-RGD released in peripheral organs. Unfortunately, there are no syngeneic glioma lines in these animals; thus, the efficacy of hMSC-Δ24 in gliomas, the focus of this report, cannot be assessed in these animals. Nevertheless, our mouse models allowed for assessments of toxicity associated with delivering hMSCs intravascularly. Carotid injection resulted in hMSCs in the lungs, implicating pulmonary emboli as possible sources of morbidity. Recent studies also reported hMSCs in the liver for 8 months after i.v. injection (34). Given that hMSC-Δ24 appear to be efficacious, future studies need to focus on the potential systemic toxicity of MSC-Δ24 in rat or hamster models.

Although promising, the results of our studies regarding clinical translation must be interpreted with some caution, as they rely on established glioma cell lines that may not completely mimic gliomas found *in situ*. Although the U251 model is more infiltrative than the U87 model, both lack extensive infiltration common to gliomas. Nevertheless, these models produce significant angiogenesis, which is important for testing intravascular delivery systems such as hMSCs. In addition, much of our previously published data on Δ24-RGD has relied on intratumoral injections of these models (2, 3); therefore, they provide references for comparing intratumoral delivery of Δ24-RGD to intravascular delivery via hMSCs. Although it may be desirable to study the effects of MSC-Δ24 in tumor models from genetically engineered mice, these approaches are not feasible because murine cells do not support adenoviral replication (see above). The recent isolation of glioma stem cells may represent an alternative model. Although these models are infiltrative, they tend to induce more limited angiogenesis, raising concerns about their application in testing intravascular delivery strategies, such as hMSCs. Nevertheless, testing of hMSC-Δ24 in these models is currently under investigation.

Disclosure of Potential Conflicts of Interest

No potential conflicts of interest were disclosed.

Acknowledgments

Received 10/7/08; revised 8/27/09; accepted 9/10/09; published OnlineFirst 11/17/09.

Grant support: Clinician Investigator Program of the Royal College of Physicians and Surgeons of Canada (R.L. Yong); National Cancer Institute grants R01 CA115729 and P50 CA 127001 (F.F. Lang), CA-1094551 and CA-116199 (F.C. Marini), and CA-55164, CA-16672, and CA-49639 (M. Andreeff); M. D. Anderson Center for Targeted Therapy, National Brain Tumor Foundation, Elias Family Fund for Brain Tumor Research, Gene Pennebaker Brain Cancer Fund, Brian McCullough Research Fund, and Run for the Roses Foundation (F.F. Lang); and Susan G. Komen Breast Cancer Foundation (F.C. Marini).

M. Andreeff is Paul and Mary Haas Chair in Genetics.

The costs of publication of this article were defrayed in part by the payment of page charges. This article must therefore be hereby marked *advertisement* in accordance with 18 U.S.C. Section 1734 solely to indicate this fact.

We thank Drs. Ayguen Sahin and Bob Carter (Harvard Medical School) for providing us with U87MG-LucNeo.

References

1. Stupp R, Mason WP, van den Bent MJ, et al. Radiotherapy plus concomitant and adjuvant temozolomide for glioblastoma. N Engl J Med 2005;352:987–96.
2. Fueyo J, Gomez-Manzano C, Alemany R, et al. A mutant oncolytic adenovirus targeting the Rb pathway produces anti-glioma effect *in vivo*. Oncogene 2000; 19:2–12.
3. Fueyo J, Alemany R, Gomez-Manzano C, et al. Preclinical characterization of the antiglioma activity of a tropism-enhanced adenovirus targeted to the retinoblastoma pathway. J Natl Cancer Inst 2003;95:652–60.
4. Krasnykh V, Dmitriev I, Mikheeva G, Miller CR, Belousova N, Curiel DT. Characterization of an adenovirus vector containing a heterologous peptide epitope in the HI loop of the fiber knob. J Virol 1998;72:1844–52.
5. Dmitriev I, Krasnykh V, Miller CR, et al. An adenovirus vector with genetically modified fibers demonstrates expanded tropism via utilization of a coxsackievirus and adenovirus receptor-independent cell entry mechanism. J Virol 1998;72:9706–13.
6. Chiocca EA, Abbed KM, Tatter S, et al. A phase I open-label, dose-escalation, multi-institutional trial of injection with an E1B-Attenuated adenovirus, ONYX-015, into the peritumoral region of recurrent malignant gliomas, in the adjuvant setting. Mol Ther 2004;10:958–66.
7. Lang FF, Bruner JM, Fuller GN, et al. Phase I trial of adenovirus-mediated p53 gene therapy for recurrent glioma: biological and clinical results. J Clin Oncol 2003;21: 2508–18.
8. Kirn D. Clinical research results with dl1520 (Onyx-015), a replication-selective adenovirus for the treatment of cancer: what have we learned? Gene Ther 2001;8:89–98.
9. Alemany R, Suzuki K, Curiel DT. Blood clearance rates of adenovirus type 5 in mice. J Gen Virol 2000;81:2605–9.
10. Lieber A, He CY, Meuse L, et al. The role of Kupffer cell activation and viral gene expression in early liver toxicity after infusion of recombinant adenovirus vectors. J Virol 1997;71:8798–807.
11. Nakamizo A, Marini F, Amano T, et al. Human bone marrow-derived mesenchymal stem cells in the treatment of gliomas. Cancer Res 2005;65:3307–18.
12. Nakamura K, Ito Y, Kawano Y, et al. Antitumor effect of genetically engineered mesenchymal stem cells in a rat glioma model. Gene Ther 2004;11:1155–64.
13. Digirolamo CM, Stokes D, Colter D, Phinney DG, Class R, Prockop DJ. Propagation and senescence of human marrow stromal cells in culture: a simple colony-forming assay identifies samples with the greatest potential to propagate and differentiate. Br J Haematol 1999;107:275–81.
14. Colter DC, Class R, DiGirolamo CM, Prockop DJ. Rapid expansion of recycling stem cells in cultures of plastic-adherent cells from human bone marrow. Proc Natl Acad Sci U S A 2000;97:3213–8.
15. Hall B, Dembinski J, Sasser AK, Studeny M, Andreeff M, Marini F. Mesenchymal stem cells in cancer: tumor-associated fibroblasts and cell-based delivery vehicles. Int J Hematol 2007;86:8–16.
16. Studeny M, Marini FC, Champlin RE, Zompetta C, Fidler IJ, Andreeff M. Bone marrow-derived mesenchymal stem cells as vehicles for interferon-β delivery into tumors. Cancer Res 2002;62:3603–8.
17. Studeny M, Marini FC, Dembinski JL, et al. Mesenchymal stem cells: potential precursors for tumor stroma and targeted-delivery vehicles for anticancer agents. J Natl Cancer Inst 2004;96:1593–603.
18. Klopp AH, Spaeth EL, Dembinski JL, et al. Tumor irradiation increases the recruitment of circulating mesenchymal stem cells into the tumor microenvironment. Cancer Res 2007;67:11687–95.
19. Komarova S, Kawakami Y, Stoff-Khalili MA, Curiel DT, Pereboeva L. Mesenchymal progenitor cells as cellular vehicles for delivery of oncolytic adenoviruses. Mol Cancer Ther 2006;5:755–66.
20. Stoff-Khalili MA, Rivera AA, Mathis JM, et al. Mesenchymal stem cells as a vehicle for targeted delivery of CRAds to lung metastases of breast carcinoma. Breast Cancer Res Treat 2007;105:157–67.
21. Hakkarainen T, Sarkioja M, Lehenkari P, et al. Human mesenchymal stem cells lack tumor tropism but enhance the antitumor activity of oncolytic adenoviruses in orthotopic lung and breast tumors. Hum Gene Ther 2007;18:627–41.
22. Sonabend AM, Ulasov IV, Tyler MA, Rivera AA, Mathis JM, Lesniak MS. Mesenchymal stem cells effectively deliver an oncolytic adenovirus to intracranial glioma. Stem Cells 2008;26:831–41.
23. Rubin JB, Kung AL, Klein RS, et al. A small-molecule antagonist of CXCR4 inhibits intracranial growth of primary brain tumors. Proc Natl Acad Sci U S A 2003;100: 13513–8.
24. Szentirmai O, Baker CH, Lin N, et al. Noninvasive bioluminescence imaging of luciferase expressing intracranial U87 xenografts: correlation with magnetic resonance imaging determined tumor volume and longitudinal use in assessing tumor growth and antiangiogenic treatment effect. Neurosurgery 2006;58:365–72, discussion 372.
25. Olmsted-Davis EA, Gugala Z, Gannon FH, et al. Use of a chimeric adenovirus vector enhances BMP2 production and bone formation. Hum Gene Ther 2002;13: 1337–47.
26. Lal S, Lacroix M, Tofilon P, Fuller GN, Sawaya R, Lang FF. An implantable guide-screw system for brain tumor studies in small animals. J Neurosurg 2000;92: 326–33.
27. Fidler IJ, Schackert G, Zhang RD, Radinsky R, Fujimaki T. The biology of melanoma brain metastasis. Cancer Metastasis Rev 1999;18:387–400.
28. Conget PA, Minguell JJ. Adenoviral-mediated gene transfer into *ex vivo* expanded human bone marrow mesenchymal progenitor cells. Exp Hematol 2000;28: 382–90.
29. Ruster B, Gottig S, Ludwig RJ, et al. Mesenchymal stem cells display coordinated rolling and adhesion behavior on endothelial cells. Blood 2006;108:3938–44.
30. Segers VF, Van Riet I, Andries LJ, et al. Mesenchymal stem cell adhesion to cardiac microvascular endothelium: activators and mechanisms. Am J Physiol Heart Circ Physiol 2006;290:H1370–7.
31. Steingen C, Brenig F, Baumgartner L, Schmidt J, Schmidt A, Bloch W. Characterization of key mechanisms in transmigration and invasion of mesenchymal stem cells. J Mol Cell Cardiol 2008;44:1072–84.
32. Bauerschmitz GJ, Kanerva A, Wang M, et al. Evaluation of a selectively oncolytic adenovirus for local and systemic treatment of cervical cancer. Int J Cancer 2004; 111:303–9.
33. Alonso MM, Gomez-Manzano C, Bekele BN, Yung WK, Fueyo J. Adenovirus-based strategies overcome temozolomide resistance by silencing the O^6-methylguanine-DNA methyltransferase promoter. Cancer Res 2007;67:11499–504.
34. Vilalta M, Degano IR, Bago J, et al. Biodistribution, long-term survival, and safety of human adipose tissue-derived mesenchymal stem cells transplanted in nude mice by high sensitivity non-invasive bioluminescence imaging. Stem Cells Dev 2008;17:993–1003.